Ultrafast 2D-IR spectroscopy of intensely optically scattering pelleted solid catalysts

(F)

(iD) **Paul M. Donaldson,** (iD) **Russell F. Howe,** (iD) **Alexander P. Hawkins, et al.**

COLLECTIONS

Paper published as part of the special topic on Celebrating 25 Years of Two-dimensional Infrared (2D IR) Spectroscopy

(F) This paper was selected as Featured

View Online   Export Citation   CrossMark

ARTICLES YOU MAY BE INTERESTED IN

Ultrafast 2D-IR spectroscopy of intensely optically scattering pelleted solid catalysts Ⓕ

View Online   Export Citation   CrossMark

Paul M. Donaldson,[1,a)] ⓘD Russell F. Howe,[2] ⓘD Alexander P. Hawkins,[1] ⓘD Mike Towrie,[1]
and Gregory M. Greetham[1] ⓘD

AFFILIATIONS

[1] Central Laser Facility, Research Complex at Harwell, STFC Rutherford Appleton Laboratory, Harwell Science and Innovation
Campus, Didcot OX11 0QX, United Kingdom
[2] Department of Chemistry, University of Aberdeen, Aberdeen AB24 3UE, United Kingdom

Note: This paper is part of the JCP Special Topic on Celebrating 25 Years of Two-Dimensional Infrared (2D IR) Spectroscopy.
a)Author to whom correspondence should be addressed: paul.donaldson@stfc.ac.uk

ABSTRACT

Solid, powdered samples are often prepared for infrared (IR) spectroscopy analysis in the form of compressed pellets. The intense scattering of incident light by such samples inhibits applications of more advanced IR spectroscopic techniques, such as two-dimensional (2D)-IR spectroscopy. We describe here an experimental approach that enables the measurement of high-quality 2D-IR spectra from scattering pellets of zeolites, titania, and fumed silica in the OD-stretching region of the spectrum under flowing gas and variable temperature up to ~500 °C. In addition to known scatter suppression techniques, such as phase cycling and polarization control, we demonstrate how a bright probe laser beam comparable in strength with the pump beam provides effective scatter suppression. The possible nonlinear signals arising from this approach are discussed and shown to be limited in consequence. In the intense focus of 2D-IR laser beams, a free-standing solid pellet may become elevated in temperature compared with its surroundings. The effects of steady state and transient laser heating effects on practical applications are discussed.

INTRODUCTION

The development of a physical and chemical understanding of solid heterogeneous catalysts is of great practical importance. In order to gain a molecular-scale understanding of heterogeneous catalysts and their properties, many investigations draw on measurement approaches involving spectroscopy, diffraction, imaging, and mass analysis.[1,2] Of these, infrared (IR) spectroscopy plays an important role.[3–5] IR spectroscopy is widely available, uses relatively compact and inexpensive instrumentation, and gives numerous spectra–structure correlations providing bond-specific information for identifying adsorbed molecular species, surface–adsorbate interactions, catalyst state, and catalyst purity. The ability to monitor these properties *in situ* makes IR spectroscopy a powerful probe of catalysis and catalyst behavior. There are numerous sampling techniques suitable for measuring the different forms that heterogeneous catalysts take under controlled temperature and loading conditions, such as diffuse reflectance from powders, transmission through pressed pellets, reflection-absorption from single crystal surfaces, and attenuated total reflectance from thin films or suspensions.[6]

When IR spectroscopy is an appropriate choice for characterizing a particular catalyst, challenges that might be encountered include the assignment of spectral features, the deconvolution of multiple overlapping bands, and the extraction of structural and dynamical information from spectral line shapes. These issues can reduce the accuracy and applicability of IR applications to catalysis research, as well as adding time and cost to investigations. Similar to the extension of nuclear magnetic resonance spectroscopy to higher frequency dimensions, the pulsed IR-analog, two-dimensional (2D)-IR spectroscopy,[7,8] can add value to IR investigations of catalysts by solving some of the above problems. This paper addresses the challenge of applying 2D-IR spectroscopy to investigations of powdered catalysts in pressed solid

form, where scattering of the IR laser light used as part of generating 2D-IR spectra into the detectors typically overwhelms the measurement.

2D-IR spectroscopy involves the excitation of two vibrational states by a sequence of laser pulses. These could be the same vibrational mode excited twice ("diagonal peaks") or the excitation of two different vibrational modes to give an off-diagonal signal ("cross-peaks"). 2D-IR spectra are 3D plots of the dependence of the emission from the sample as a function of two frequencies. These are frequencies of excitation (pumping) and emission (probing) and are denoted here as ω_1 and ω_3. Vibrational features in a 2D-IR spectrum commonly consist of pairs of peaks corresponding to different possible permutations of the two-state laser excitation steps. The frequency separation of each peak pair in a 2D-IR spectrum depends on anharmonic terms describing the potential energy surfaces of the vibrational modes and the character of the vibrational modes (e.g., local mode, normal mode, exciton, Fermi resonance, etc.). 2D-IR spectroscopy of the diagonal bands provides a powerful probe of the origins of the IR absorption line shape. The component of line shape broadening caused by different molecular structural configurations (inhomogeneous broadening) determines the diagonal width of 2D-IR peaks. Processes affecting the IR line shape but occurring faster than the timescale of the 2D-IR measurement, such as fast structural dynamics and population relaxation (homogeneous broadening), control the diagonal 2D-IR peak's anti-diagonal width.[9,10] The diagonal peaks of 2D-IR spectra may evolve as a function of the time delay between pumping and probing pulses. This "waiting time" (t_2) may extend across the range of ~20 fs–200 ps for a given molecular system. Through waiting time dependence, 2D-IR line shapes can be time-resolved to obtain the rates of a molecule's structural evolution.[11–13] Time resolution can also be used to examine rotational dynamics[14] and vibrational energy transfer.[15]

2D-IR spectroscopy is most commonly performed in transmission geometries on transparent samples, with surface reflection and surface attenuated total reflection (ATR) geometries also feasible.[8] When samples are not perfectly transparent, the intense IR pump laser light used as part of determining a 2D-IR spectrum is scattered toward the detector. For relatively transparent samples, the scattered light produces unwanted spectral features that can be removed using data collection techniques involving chopping, optical phase cycling, and polarization control.[16–22] For powdered solid samples such as those studied in this manuscript, the scatter signals and their accompanying noise dominate the desired 2D-IR signals. To enable 2D-IR studies of powdered solid samples normally too scattering to detect a 2D-IR signal from, one approach has been to use dispersions of the powders in index matching oil. This method has been used to study gypsum, metal-organic-frameworks (MOFs), and zeolite ZSM-5.[23–25] Index matching substantially reduces the scatter levels but adds an undesirable preparation step, a potential source of contaminant and complications to temperature-dependent loading and desorption studies of catalysts. In one counter example, a relatively low scattering MOF (as indicated by its FT-IR spectrum) with strong 2D-IR signal intensities of organic metal carbonyl guest molecules did permit a 2D-IR study of the samples as a dry powder without the need for an index-matching medium.[26] Several decades ago, prior to the development of 2D-IR techniques, hydroxyl lifetime and line shape studies of optically scattering zeolites using two-color IR-pump-probe spectroscopy were reported.[27,28] Given the low time

resolution (30 ps), low repetition rate lasers, and single channel detectors used, the scope of these studies and quality of the spectra are remarkable. The narrow laser width and ease of demodulating the signal from the probe and scattered light probably explain the successful elimination of scatter from these measurements.

In this paper, we report on how to acquire high-quality 2D-IR spectra from intensely scattering powdered samples compressed into thin pellets under controlled temperature and buffer gas composition. For 2D-IR experiments in the pump-probe geometry, in order to enable the study of strongly scattering samples, we use a bright probe beam comparable in strength with the pump fields. Suppression of the scattered pump light goes in proportion to the increase in probe brightness. Scatter signals involving the interference between the scattered pump light and the probe ("heterodyne scatter") are suppressed as the square root of the increase in probe light and then eliminated by pump phase cycling. We will show that the combination of bright probe and phase cycling enables 2D-IR spectra of pelleted zeolites to be collected with parallel polarization of the pump and probe fields. Measuring with perpendicular polarization of the pump and probe fields eliminates most of the diagonal scatter from the samples examined. Under parallel polarization, the amount of diagonal scatter can be reduced to the levels where off-diagonal spectral regions are unaffected by the scatter. We also discuss laser heating effects relevant to the study of free-standing solids in a gas cell and comment on the nonlinear effects that might arise from using a probe field of similar intensity to the pump fields. We conclude that these are qualitatively indistinguishable from those caused by strong pump field effects.

METHODS

Samples

P25 TiO_2 (a 70% anatase 30% rutile composite) and fumed silica were obtained from Sigma-Aldrich. Zeolite Y (proton form, silicate to aluminate ratio of 5), and ZSM-5 (ammonium form, silicate to aluminate ratio 50) were obtained from Zeolyst. The ammonium form of ZSM-5 was converted to the proton form by calcination in air at 600 °C for 12 h. Pellets of each sample were made in a hydraulic press (Specac) using a 13 mm diameter die containing 7–20 mg of material and a pressure of 2 tonnes applied for 1 min. The self-supporting pellets were 70–120 μm in thickness and presented for 2D-IR experiments in one of two spectroscopy cells: (1) the pellets were contained between 2 mm CaF_2 windows spaced by a 0.5 mm thick Teflon ring split into two pieces to allow gas flow in and out. These were placed within a sealed, temperature controllable spectroscopy cell (Harrick, TFC-S25-3, 220 °C maximum temperature) with a gas inlet/outlet. (2) The pellet was mounted onto the heater block of a spectroscopy cell using a thin steel ring as a clamp (Linkam, FTIR600). A 4 mm hole drilled through the middle of the heater block allowed light to pass through the pellet. The heating block was not in contact with the 0.5 mm thick CaF_2 windows attached to the cell body to seal the cell, allowing a maximum block temperature of 600 °C to be achieved. Both types of cells were operated at 1 atm pressure under constant flowing N_2 carrying controlled amounts of D_2O vapor, obtained by sparging N_2 through D_2O in a Dreschel flask and diluting the vapor saturated flow in dry N_2.
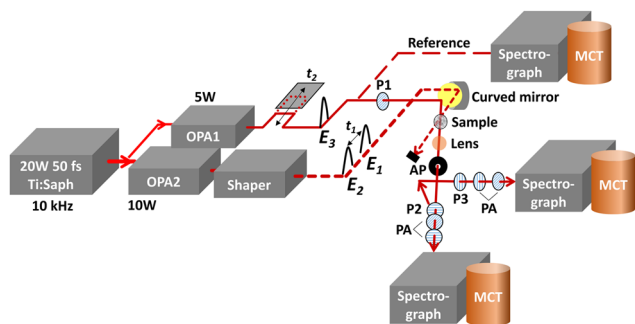
FIG. 1. 2D-IR spectrometer layout: P = polarizer (wire grid), PA = polarizer-attenuator (pair of wire grid polarizers), AP = aperture, MCT = HgCdTe detector array (128 pixels for probes and 32 pixels for reference).
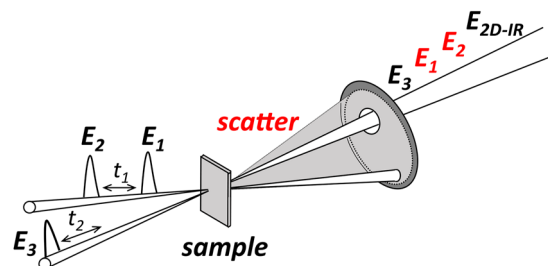

FIG. 2. 2D-IR spectroscopy in the three-pulse pump-probe geometry and the nomenclature used for labeling incident fields E, time delays under experimental control t, scatter, and signal. Pulse 2 is fixed in time. Fields from the transmitted beams are denoted in black font and fields of scattered light shown in red font.

Spectroscopy

A 2D-IR spectrometer built at the Central Laser Facility (STFC Rutherford Appleton laboratory, UK) was used to study microcrystalline-pelleted samples. The layout is shown in Fig. 1. A Ti:Sapphire amplifier system (Coherent Legend Elite Duo) produced 20 W, 10 kHz, 50 fs, and 800 nm pulses. This output pumped two Optical Parametric Amplifiers (OPAs) to act as separate pump and probe sources, generating mid-IR light centered at around 2600–2650 cm^{-1}. Pulse energies at source ranged from 1.5 to 2.5 μJ (probe) and 2–3 μJ (pump). Full width at half height (FWHH) spectral bandwidths were 350–450 cm^{-1} (probe) and 200–250 cm^{-1} (pump). The output of the pump OPA was passed through a 4f Ge acousto-optic pulse shaper (Phasetech Spectroscopy). At the sample, incident pulse energies were around 0.5–1.5 μJ (probe) and 0.2–1 μJ (pump, depending on the pulse shaper mode).

The 2D-IR spectrometer operated in the three-pulse pump-probe geometry (see Figs. 1 and 2), where the collinear pair of excitation pulses E_1 and E_2 generated by the pulse shaper constitute the "pump" beam. A third, non-collinear beam of pulses E_3 is used for both signal generation and heterodyne detection of the signal and is referred to as the "probe" beam. The two beams of pump

and probe light were focused into the sample with a 10 cm focal length off-axis parabolic mirror, and an IR camera used to optimize their spatial overlap.[29] Typical spot sizes were 40–50 μm FWHH. The pump and probe beams propagated collinearly toward the off-axis parabolic mirror ~20 mm in distance from one another. The angle between the two beams was, therefore, ~12°. The probe light diverging from the sample position was collimated using a 10 cm focal length ZnSe lens and passed through an aperture of 3–4 mm (the size of the unfocussed probe beam), which served to reject some of the scattered pump light. All polarizers used were of the wire grid type (Thorlabs, CaF$_2$, BaF$_2$, or ZnSe substrates). In order to measure parallel and perpendicular components of the pump-probe 2D-IR signal ($\langle XXXX \rangle$ and $\langle XXYY \rangle$), a wire grid polarizer polarized the sample-incident probe light at an angle of 45° to the pump light (P1, Fig. 1). After the sample, a second wire grid polarizer (P2, Fig. 1) separated the component of the probe parallel to the pump from the perpendicularly polarized component. Both components were measured on separate detectors simultaneously. An additional polarizer was used to remove residual perpendicular polarized light from the parallel beam (P3, Fig. 1). Pairs of wire grid polarizers (marked PA on Fig. 1) were used to both attenuate the probe light prior to detection and to maintain the same polarization into the spectrographs. The parallel and perpendicular probe beams were dispersed
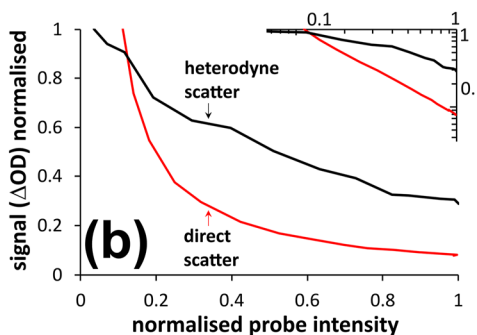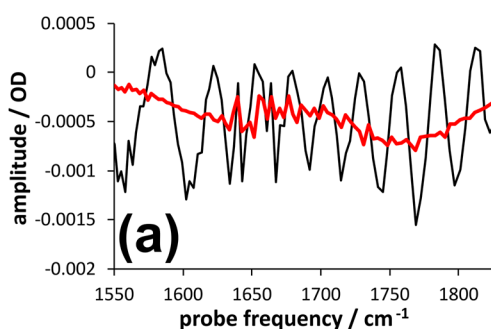
FIG. 3. Direct and heterodyne pump scatter contributions to a pump-probe signal depend on probe intensity. A scratched CaF$_2$ window at the sample position of a 2D-IR spectrometer was used to scatter pump light toward the detector. In (a), the black line is the total scatter observed. The direct scatter (red line) is isolated by phase cycling. In (b), the amplitudes of the heterodyne scatter and direct scatter are plotted as a function of sample-incident probe intensity. The oscillatory heterodyne scatter signal amplitude was isolated from the direct scatter by Fourier transform. The inset shows the main plot with logarithmic axes. $t_2 = 1$ ps.

in individual spectrometers onto separate HgCdTe array detectors (Infrared Associates, 128 pixels) at ~4 cm^{-1} probe spectral resolution per pixel. IR spectral intensities were digitized shot-by-shot (Infrared Development Systems FPAS), and simultaneous probe reference intensity measurements recorded using a small amount of pre-sample probe light were sent to a separate spectrometer/detection system. The reference intensity fluctuations measured were used to correct the 2D-IR measurements using a correlation method similar to that introduced by Feng *et al.*[30] Spectrally dispersed Kerr responses from CaF$_2$ as a function of pump-probe delay were observed by rotating polarizer P2 (Fig. 3) to a state almost perpendicular to the probe beam. The dispersed Kerr responses were used to determine the levels of dispersion compensation required for the pump beam (controlled by the pulse shaper) and the probe beam (controlled by the elimination of unnecessary optical elements). Over the course of many experiments, response times of 90–120 fs full width half height (FWHH) were achieved.

2D-IR spectra were generated by Fourier transform (FT) of spectral interferograms acquired using t_1 scans in steps of 17–22 fs to the final times of 3–4 ps, with the smaller value of the final time used for improved signal to noise and the larger used for slightly better localization of diagonal scatter and thermal artifacts. Four-frame phase cycling and a bright probe were used for scatter suppression, as described in the "Results" section. The data acquisition and experiment control system were LabVIEW based. FT-IR spectra were collected using a Bruker Tensor at 4 cm^{-1} spectral resolution.

RESULTS AND DISCUSSION

Scattered light in the three-pulse pump-probe geometry for 2D-IR spectroscopy

The basic scheme and nomenclature for 2D-IR spectroscopy in the pump-probe geometry are shown in Fig. 2. We shall refer to this common way of collecting a 2D-IR spectrum as "three-pulse" pump-probe 2D-IR. By using non-collinear excitation beam geometries such as the three-pulse pump-probe or related four wave mixing "boxcars" geometry for 2D-IR spectroscopy,[7] the powerful IR excitation fields required to generate measurable signals are terminated out of the line of sight of the IR detectors. Although, in principle, no light other than the 2D-IR signal and probe field/local oscillator reaches the IR detectors, in-practice, even for transparent samples, imperfections in the sample cell window surfaces, undissolved samples, and suspended impurities cause small amounts of pump light to be scattered toward the detector (Fig. 2). Light scattering effects appear as an unwanted signal in the diagonal region of a 2D-IR spectrum. As scatter levels increase, their associated intensity noise contribution to t_1 interferograms cause increasing amounts of noise at all frequencies of the Fourier Transformed (FT) 2D-IR spectrum, obscuring the 2D-IR signal.

Contributions of scattering to a three-pulse pump-probe 2D-IR spectrum may be assessed by considering the possible electric field contributions E to the total measured intensity ($I \propto E^2$) at a given detection frequency (detector pixel) ω_3. We consider scattered fields from laser pulses 1 and 2 interfering at the detector with pulsed field 3 (probe) and the 2D-IR signal field (Fig. 2). To illustrate the essential behavior of the 2D-IR signal and scatter, for simplicity, we consider the signal recovery procedure of shot-by-shot

measurement of the total intensity with the pump fields modulated on and off (chopped, $S_{total} = -\log[I_{on}/I_{off}]$). Similar expressions can be derived for phase cycling. From the well-known superposition/interference properties of electric fields, a simplified representation of the properties of the measured 2D-IR signal and the scatter is readily deduced,

$$S_{total} \approx -\log\Big[\big(E_3^2 + E_1^2 + E_2^2 + \boldsymbol{E_3 E_{2D-IR}} + a_{31}E_3 E_1 + a_{32}E_3 E_2 + \boldsymbol{a_{12}E_1 E_2}\big)/E'^2_3\Big], \quad (1)$$

$$a_{ij} = \cos(\omega_3 t_{ij} + \varphi_{ij}) \quad (2)$$

Δt and Δφ are the time and phase differences between each pulsed field. i and j label pulse 1, 2, or 3. In the three-pulse pump-probe geometry, the 2D-IR signal depends on the incident field strengths, pulse delays, and phases as

$$E_{2D-IR} \propto E_1 E_2 E_3 \, \cos(\varphi_{12}) M(t_1, t_2, \omega_3). \quad (3)$$

φ_{12} is the phase difference between fields 1 and 2. Here, $M(t_1,t_2,\omega_3)$ contains the interferogram that is transformed to a 2D-IR spectrum and other remaining factors affecting the 2D-IR signal.

2D-IR spectra are computed by Fourier transform of the changes in the total measured signal at each probe wavelength value as a function of coherence time t_1 for fixed waiting time t_2. In Eq. (1), the terms *not* in bold will not appear in a 2D-IR spectrum after Fourier transform because they do not depend on t_1. They will only contribute to the Fourier transform at zero frequency. Owing to the relatively large size of the probe intensity E_3^2 at the detector, however, its noise fluctuations appear in the 2D-IR spectrum at all Fourier frequencies. The same is true when the scatter terms are very large. In Eq. (1), a separate measurement (E'^2_3) is made for normalization with the pump beams blocked (chopped). This also eliminates the E_3 spectral amplitude dependence in Eq. (3) from the heterodyned 2D-IR signal $E_3 E_{2D-IR}$. Even under intense pump scattering, $E_3 > E_1 + E_2 > E_{2D-IR}$; hence, the contributions of the cross-terms between the 2D-IR signal field and fields 1 and 2 are neglected from Eq. (1), as is the quadrature 2D-IR signal. A contrasting situation where the former is not true would be 2D-IR approaches using collinear beams, such as gas-phase waveguide 2D-IR[31] and 2D-IR spectro-microscopy.[32]

In a pump-probe geometry 2D-IR experiment, there are two types of components of scattered light from Eq. (1) that are t_1 dependent and, therefore, appear in a 2D-IR spectrum. We define these here as *direct scattered* pump light ($E_1 E_2$) and *heterodyned scatter* ($E_3 E_1$). Direct scattering is simply the pump light that reaches the detector. Heterodyne scatter is the interference of pump and probe fields at the detector. Both types of scatter signals appear along the diagonal of the 2D-IR spectrum with a width defined by the experimental spectral resolution (set by the longest t_1 time acquired and by the probe spectrometer resolution). Heterodyned scatter signals contributing to interferograms collected as a function of t_1 are modulated by the factor $\cos(\omega_3 t_{13})$, where $t_{13} = t_1 + t_2$ - the time delay between pulses 1 and 3. The appearance of the heterodyne scatter in a 2D-IR spectrum, therefore, includes a modulation in amplitude along the diagonal that is dependent on t_2. Direct scatter signals

are modulated by a factor $\cos(\omega_3 t_1)$ and appear on the diagonal of a 2D-IR spectrum as a purely negative signal with an amplitude determined by the spectral intensity of the scattered light and wavelength dependence of the scatter and its detection. Owing to field E_3 also being the probe (heterodyning) pulse, and directly illuminating the detector, the heterodyne scatter term should, in principle, be larger in magnitude than the direct pump scatter. In practice, for the scattering samples studied here, we observed that the ratios of heterodyne and direct scatter were variable and very sensitive to the 3D positioning of the pelleted sample in the focus of the IR laser beams. We provide further reasoning behind this observation in supplementary material, Sec. 1.

For the recovery of any weak signal from a strong background, the noise of the background disproportionately affects signal to noise. Optical scattering of laser radiation from objects rough on the scale of the wavelength of light produces complex diffraction/speckle patterns in the far field that will translate to fluctuations in the measured intensity at the detector under laser pointing fluctuations and sample movements. Pulses 1 and 3 generating the heterodyned scatter are also not phase locked—the beams propagate to the sample on separate optical paths, contributing to an unstable spectral phase. It is, therefore, important for the recovery of a weak 2D-IR signal from the stronger scattered pump contributions of a heavily scattering sample that the measurement is conducted at the highest data rate and with the fastest (shot-to-shot) modulation of the beams. The mid-IR laser sources used should operate at the lowest feasible noise. Pulse-to-pulse energy/pointing correlations are often better the higher the repetition rate of the laser source.[33]

Various approaches for eliminating or reducing scattered light signals in both three-pulse pump-probe and boxcars 2D-IR experimental geometries have been discussed in the literature.[16–24,26] Modulation of excitation beam phases, delays, or amplitudes is always an essential ingredient. In the pump-probe geometry, the use of orthogonally polarized pump and probe fields and the placement of a polarizer to block the scattered pump light in front of the detector is common. The use of a mid-IR pulse shaper in the pump-probe geometry[17] allows for shot-to-shot modulation of the phases of fields 1 and 2 at laser repetition rates as high as 100 kHz.[34–36] Inspecting Eqs. (1)–(3), the heterodyned scatter term can be eliminated exactly by phase-cycling fields 1 and 2 in the sequence of four-"frames" (pulse shaper waveforms) and summing the measured intensities $I(\varphi_1, \varphi_2)$ as[7]

$$S_{phase\ cycle} = -\log[I(0,0) - I(0,\pi) + I(\pi,\pi) + I(\pi,0)]. \quad (4)$$

The direct scattered pump light ($E_1 E_2$) is not removed from the total signal by this form of phase cycling. An option for isolating and subtracting this term is to phase-cycle *and* amplitude modulate the probe beam with an optical chopper. Demonstrated previously using 1 kHz laser pulse rates,[23,32] at the higher laser repetition rates used here the IR detector electronics did not respond quickly enough to the large changes in shot-to-shot incident intensity, resulting in a disproportionate increase in noise observed in 2D-IR spectra recorded at 10 kHz. We also disfavor optical chopping because the 2D-IR signal is only measured for half of the time, increasing the measurement time required by at least a factor of two compared with pure phase cycling methods.

Reduction of light scattering in 2D-IR spectra using a bright probe beam

In the three-pulse pump-probe geometry, the contribution of the 2D-IR signal to the total signal size in Eq. (1) does not vary with probe intensity. The probe intensity dependence cancels between Eq. (1) [or the equivalent expression from Eq. (4)] and Eq. (3). For scattering however, an increase in probe intensity by a factor of n decreases the heterodyne ($E_3 E_1$) and direct scatter ($E_2 E_1$) term contributions to the total signal in Eq. (1) by factors $\sqrt{n}$ and n, respectively. Thus, a strategy for reducing the scattered light contribution to 2D-IR spectra is simply to increase the probe intensity on the sample, attenuating the probe and scattered light prior to illuminating the detector. This is demonstrated experimentally in Fig. 3 for scatter from a scratched optical window at the sample position of the 2D-IR spectrometer. The contribution of the scattered pump light to the probe spectrum is shown in Fig. 3(a) as a pump-probe signal. The plot is in absorbance units (relative to the probe intensity), as is typical in a pump-probe measurement. In Fig. 3(a), the direct scatter is separated from the oscillatory ($t_2 = 1$ ps) heterodyne scatter by using phase-cycling [see supplementary material, Sec. 3, Eq. (S1)]. The spectrally integrated signal sizes of the direct and heterodyne scatter are plotted against the measured probe intensity in Fig. 3(b). The sample-incident probe intensity was normalized to the value at detector maximum (1 = saturation) and controlled using a motorized wire-grid polarizer pair attenuator. The scatter signals are normalized to their highest observed value. Figure 3(b) shows that the direct scatter is more strongly suppressed than the heterodyne scatter on increasing the probe intensity. A logarithmic plot [Fig. 3(b) inset] clearly shows that as expected, the attenuation of the heterodyne scatter goes roughly as the square-root of increasing probe intensity [the log–log plot slope is ~0.5, Fig. 3(b) inset black], and the attenuation of direct scatter is linear [the log–log plot slope is 1, Fig. 3(b) inset red].

Equations (1)–(3) and Fig. 3 put the advantages of a bright probe on a quantitative footing. In practice, the actual amount of probe and scattered pump light imaged onto the detector, and the consequent ratios of signal to scatter depend in a complex manner on the sample, laser, and spectrometer optics. Attenuation effects acting on both the pump and probe equally, such as the absorption of the sample and the efficiency of the spectrograph do not affect the outcome, although they do require a brighter probe for optimal detector illumination. As the scattering strength of the sample increases to the point where the probe intensity is diminished at the detector (e.g., for TiO_2 and zeolite Y in Fig. 4), the margin of scatter suppression with a bright probe diminishes. Even under such strong scattering, the essential conclusion is that, along with phase-cycling and polarization, probe intensity is an essential tool for the 2D-IR spectroscopist to use in reducing scatter. Our experience is that it improves not only the quality of 2D-IR data collected but also the chances of locating the pump-probe signal on the placement of the sample in the spectrometer.

Bright probe, phase-cycled 2D-IR spectroscopy of scattering samples

In this section, we demonstrate the bright probe, phase-cycled 2D-IR approach to study pressed pellets of microcrystalline
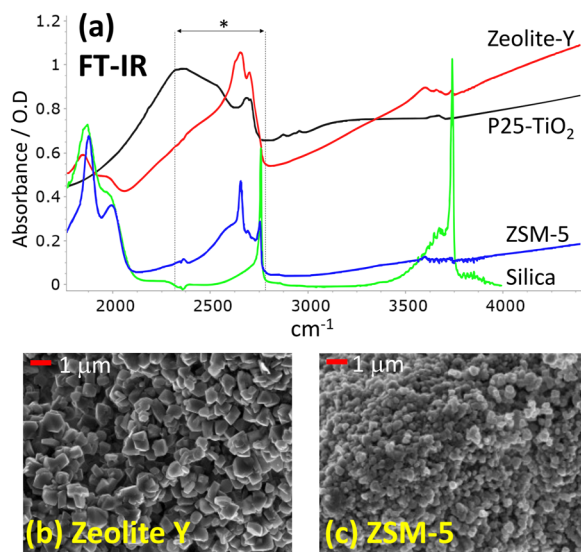
FIG. 4. (a) FT-IR spectra of pelleted zeolite Y, P25 TiO₂, ZSM-5, and fumed silica of thickness 80–120 μm held at ~200 °C and in flowing N₂/D₂O vapor.[#] The absolute absorption scale and offsets are the same for all samples, each spectrum sitting on a background due to optical scattering. The region examined in the 2D-IR experiments* is shown between the dotted lines. (b) and (c) show SEM images of the zeolite Y and ZSM-5 samples. [#]To reduce the levels of SiOD-stretch absorption, the fumed silica is in a 50/50 mix of H₂O and D₂O vapor.

samples zeolite Y, P25 TiO₂, ZSM-5, and fumed silica heated to 200 °C in flowing N₂/D₂O vapor. At 200 °C, these samples quickly become deuterated but are thought to be largely free from any bound water. We discuss the merits of studying deuterated samples in supplementary material, Sec. 2. To the naked eye, although the fumed silica was relatively translucent, the pellets of the two zeolites and P25 were opaque. Although these materials are themselves actually transparent in the visible part of the spectrum, the sub-micron scale crystals (zeolites) and nanoparticle agglomerations (TiO₂ and fumed silica) scatter light strongly. The amount of light scattered from a compressed pellet of densely packed crystals/agglomerates depends on their size distributions and refractive index relative to the medium surrounding the object. As the size of the crystals approaches the wavelength of the light and as the refractive indices of the particle and medium diverge from one another, optical scattering increases.

Figure 4 shows FT-IR spectra of all the samples examined (a) and scanning electron microscope (SEM) images of zeolite Y (b) and ZSM-5 (c). The wavelength-dependent background in the FT-IR spectra of Fig. 4(a) is due to losses of scattered light that exceed the collection angle of the spectrometer optics. This background provides a useful qualitative measure of the IR light scattering properties of the samples. The particular P25 and zeolite Y samples examined are clearly much more scattering than the ZSM-5. The fumed silica is minimally scattering. The SEM images Figs. 4(b) and 4(c) show monodisperse zeolite crystals, with average sizes of ~0.8 and ~0.3 μm for zeolite Y and ZSM-5, respectively. This explains their differing scattering strengths. P25 TiO₂ and fumed silica are not monocrystalline, and although they have primary particle sizes in the vicinity

of 25 nm, depending on preparation and handling, both form dense, highly poly disperse aggregates and agglomerates with sizes into the micrometer range.[37,38] The strong IR scattering in Fig. 4 shows that this is clearly the case for the TiO₂.

Three-pulse pump-probe geometry 2D-IR spectroscopy is normally carried out with ~10–20 nJ/pulse of probe light incident on a weakly absorbing sample—optimal for illuminating the 128 element MCT array detector used with the ~350 cm⁻¹ bandwidth mid-IR light in the present experiments. Under these levels of incident probe light, for the pellets of zeolites or TiO₂, it was not possible to identify a pump-probe signal from the scatter on placement into the spectrometer nor to recover a 2D-IR spectrum. In order to maximize the available intensity on the sample for scatter suppression by the probe, and signal generation by the pump, we used two separate OPAs for generating the pumping and probing beams (though a single OPA can also be used). The pulse energies for the probe light incident on the sample were comparable with that of the pump beam, and around 0.5–1 μJ/pulse. An estimate of the maximum possible scatter suppression possible from this increased probe intensity is, therefore, roughly, ~10× for the heterodyne component and ~50–100× for the directly scattered pump light.

Figure 5 shows 2D-IR spectra of the same pelleted samples as Fig. 4 in the OD stretch region recovered using the probe at maximal brightness on the sample, perpendicular ⟨XXYY⟩ pump-probe polarization and four-frame phase cycling [Eq. (4)]. The spectra are plotted with signals in units of mOD/Hz¹ᐟ² and a scaling accounting for the distinctions between chopping and phase cycling applied. These units come naturally from the normalization of the discrete FT data and make the signal size independent of step size and number of interferogram points.[39] To give a sense of proportion, the
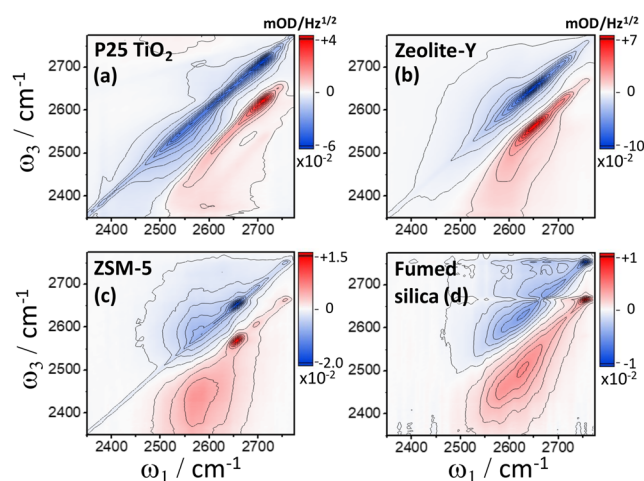

FIG. 5. 2D-IR spectra in the OD stretch region of the four-pelleted solid samples of Fig. 4(a). Blue contours are negative signals, and red contours are positive signals. The spectra are averages of 500–1000 s at a waiting time t_2 and maximum scanned coherence time t_1 of $t_2 = 0.4$ and $t_1 = 3$ ps [for the strong scattering samples (a) and (b)], and, $t_2 = 0.6$ and $t_1 = 4$ ps [for the weaker scattering samples (c) and (d)]. All spectra were collected with the four frame phase cycle sequence [Eq. (4)] and a bright probe. The pump and probe are perpendicularly polarized (⟨XXYY⟩). These spectra were collected from sample positions found to be minimally scattering.

scatter-free, peak-to-peak (chopped) pump-probe signal amplitudes for the ZSM-5 and zeolite Y measured in ⟨XXYY⟩ polarization were 0.4 and 1 mOD, respectively.

Figure 5 is a confirmation that the experimental arrangement of Fig. 1 generates 2D-IR spectra of excellent quality, despite the samples being in solid powder-pelleted form and optically scattering. Scatter makes a minimal contribution, and spectral features hinting at the potential scope of 2D-IR applications to these materials can be clearly seen. In Figs. 4(a) and 4(b), the dominating diagonal bleach-stimulated emission (SE, 0->1) and excited state absorption (ESA, 1->2) 2D-IR signal of the defect and framework deuteroxyl (OD) groups of TiO₂[40] and zeolite Y[3] have narrow anti-diagonal width and broad diagonal width (inhomogeneous broadening), suggesting that non-hydrogen bonded OD groups are present in these samples with a substantial distribution of site frequencies. In addition to showing several narrow bands characteristic of non-hydrogen bonded Si(OD)Al, AlOD, and SiOD,[3] the ZSM-5 and fumed silica prominently show an additional component of OD stretch signal that is broad along both the diagonal and anti-diagonal and suggestive of hydrogen bonded deuteroxyl groups. We will discuss these observations in more detail in a separate work.[41] Here, they serve the purpose of demonstrating the potential of 2D-IR spectroscopy to reveal line-shape origins of pelleted optically scattering solids of importance in catalysis.

We note that even with the improvements in signal-to-scatter ratios provided by the bright probe approach, alongside phase-cycling and crossed pump-probe polarization, for the strongly scattering samples TiO₂ and zeolite Y locating the optimum position of the sample in the laser focus to identify the required pump-probe signal from the scatter could be challenging. The procedure used is described in supplementary material, Sec. 3.

Figure 6 examines more closely P25 TiO₂ and zeolite Y, the two samples studied with the strongest scattering. Figures 6(a)–6(h) show the differences between parallel and perpendicular probe polarization and the effect of the application of four-frame phase cycling. The amounts of direct and heterodyne scatter observed in the experiment were variable with sample position; hence, these specific spectra are as much for illustrative as for quantitative purposes. The parallel and perpendicular measurements were taken simultaneously, but the parallel detection channel may well have imaged different amounts of scatter compared with the perpendicular channel. Nevertheless, polarization control using wire grid polarizers gave a ~300× reduction in the direct scattered light on the detector between ⟨XXXX⟩ and ⟨XXYY⟩ measurements for both samples. The specified extinction ratio for these polarizers is 1:150–1:300.

It can be seen from the non-scatter suppressing two-frame ("φ₂") measurement of zeolite Y [Fig. 6(a)] that polarization and the bright probe are almost sufficient for observing the ⟨XXYY⟩ 2D-IR spectrum scatter free. This is not the case for parallel measurement Fig. 6(b). Here, the 2D-IR signal is only partially visible under the oscillations caused by the heterodyne scatter. Application of four-frame ("φ₄"), heterodyne scatter-suppressing phase cycling returns a much improved ⟨XXYY⟩ 2D-IR spectrum of zeolite Y with only a very small amount of direct scatter remaining. For ⟨XXXX⟩, the 2D-IR signal in the non-scatter suppressing phase cycling measurement is barely visible. With four-frame ("φ₄"), heterodyne scatter suppressing phase cycling applied, we have a peak-2D-IR signal to peak-direct scatter ratio of ~0.18,
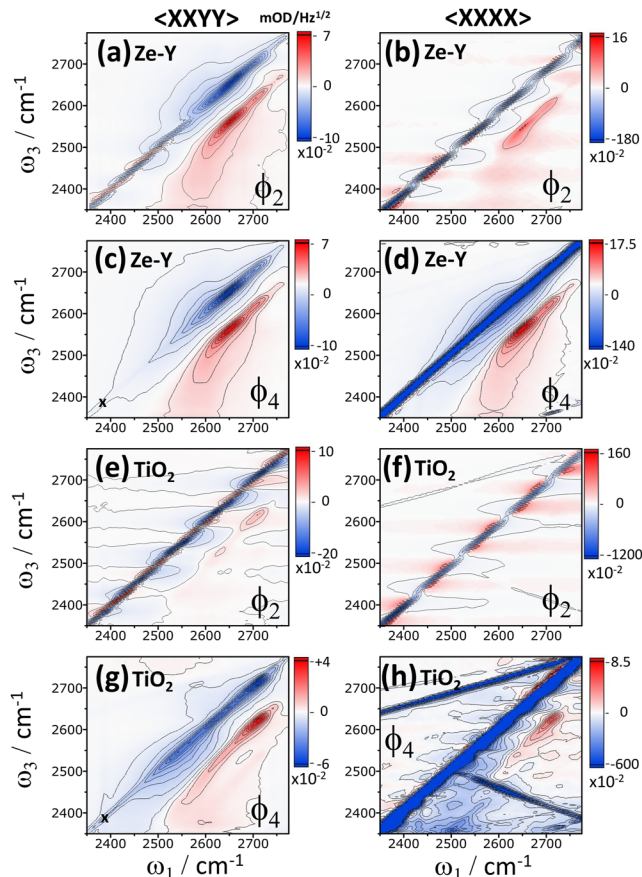

FIG. 6. 2D-IR spectra of zeolite Y (top four spectra) and TiO₂ (bottom four spectra) from Fig. 5 in perpendicular (⟨XXYY⟩, left column) and parallel (⟨XXXX⟩, right column) pump-probe polarizations, with scatter suppressing four-frame phase cycling ("φ₄") and non-scatter suppressing two-frame phase cycling ("φ₂") as indicated in each figure. The scale bars show the z-range of the 2D-IR signal in absolute units of mOD/Hz^{1/2}, correcting for the two kinds of phase cycling. In (c) and (g), the cross indicates the location where there is approximately no 2D-IR signal, only scatter. Here, the ⟨XXYY⟩ scatter levels are 0.3% of the ⟨XXXX⟩ measurement.

with the straight blue stripe along the diagonal indicating that the heterodyne scatter has been perfectly eliminated [Figs. 6(d)]. The direct scatter is perfectly contained along the diagonal, with the remaining off-diagonal 2D-IR signal captured free from the scatter with high signal to noise. Comparing the peak −ve signal sizes between zeolite Y φ₂ and φ₄ ⟨XXXX⟩ measurements Figs. 6(b) and 6(d), we see that the heterodyne signal strength is actually *weaker* than the direct scatter in this measurement by ~3.5×.

The P25 TiO₂ spectra of Fig. 6 show that despite the levels of scatter indicated by the FT-IR measurement of Fig. 4 being comparable with zeolite Y, for the pelleted sample studied, the scatter signals in the 2D-IR measurements were 4–6× higher than zeolite Y at the most optimized position for minimal scatter intensity. The 2D-IR signal in the non-scatter suppressing two-frame ("φ₂") ⟨XXYY⟩ perpendicular measurement [Fig. 6(e)] is barely visible. Application of

the four-frame phase cycle is successful in removing all of the heterodyne scatter, leaving a spectrum that has only a small amount of direct scatter along the diagonal (Fig. 6(g)). In contrast, even with four-frame phase cycling, the levels of scattered light on the detector for the parallel measurement [Fig. 6(h)] were too high for this particular sample. The oscillations indicate imperfectly subtracted heterodyne scatter. The additional off-diagonal lines are diagonal scatter generated by imperfections in the generation of pulses 1 and 2 caused by the nonlinear amplitude response[42] of the pulse shaper.

Higher-order effects

The basic definition of a pump-probe experiment requires the probe beam to be weak in order not to perturb the sample. A bright probe on the sample is a departure from this—the sample-incident pulse energies are comparable with the pump energy and interact with the sample multiple times during signal generation. In this section, we argue that for three-pulse pump-probe 2D-IR

spectroscopy, using a probe beam at an equal intensity to the pump can cause no additional nonlinearity complications than the pump itself.

2D-IR spectroscopy is third order in the total number of electric field interactions with the sample and involves two pump and a single probe ($n = 1$) field–sample interactions. Figure 7 maps out the types of diagonal 2D-IR processes that might occur in a bright probe experiment involving $n > 1$ probe interactions for pulses 1–3 properly time ordered (t_2 +ve). $n = 2$ is where the probe field supplies the second and third interactions to generate a 2D-IR signal. Using a $\langle XXYY \rangle$ polarization arrangement, the $n = 2$ signals will be $\langle XYYY \rangle$. Only $n = 2$ processes involving the scanned pump field E_1 can appear in a 2D-IR spectrum after Fourier transform. As the second and third interactions are from the probe field, the "waiting time" for these $n = 2$ 2D-IR signals is zero. The "true" experimental waiting time t_2 used to observe the desired $n = 1$ 2D-IR signal causes the $n = 2$ 2D-IR interferogram to be truncated at early coherence times t_1 and to be improperly phased. $n = 2$ processes are not phase matched in the pump-probe geometry: in the $n = 2$ diagrams
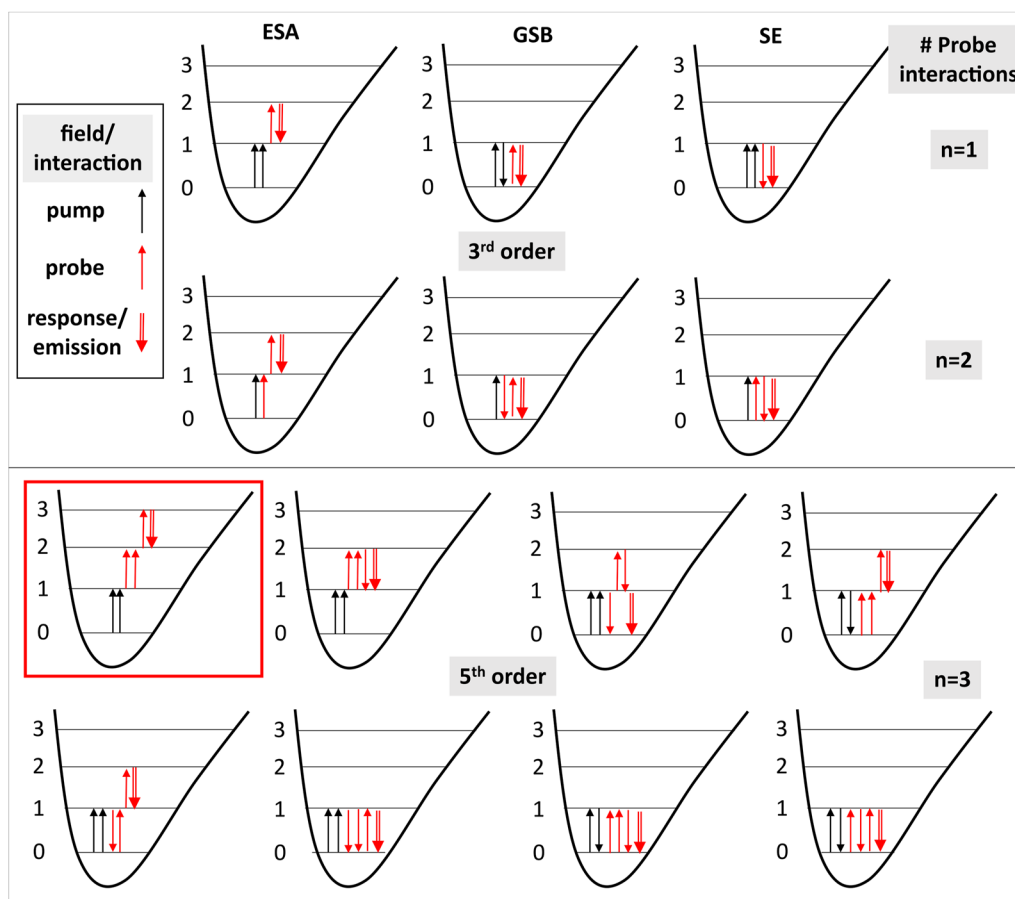

FIG. 7. The probe beam of a three-pulse pump-probe 2D-IR experiment can interact multiple times with the sample, generating various additional nonlinear signals. The energy level diagrams above depict the four states 0–3 of an anharmonic oscillator. The pump and probe field interactions are indicated by black and red arrows. The diagrams are ranked from top to bottom by the number of probe field interactions ($n = 1$–3). Nonlinear emission is depicted by a thick double red arrow. For the vibrational state "2->3" fifth-order signal, the diagram giving the clearest indication of higher-order effects in a 2D-IR spectrum is highlighted in the red box.

of Fig. 7, the first two fields from the pump and probe beams are not collinear; hence, the n = 2 2D-IR signal will radiate from the grating generated by the first two interactions into a different direction to that of the probe beam, hence mitigating the "n = 2" problem for transparent samples. If any scattered n = 2 2D-IR signal reaches the detector, it will be much weaker than the phase-matched 2D-IR signal. This would not be so if the pump and probe were collinear (as would be the case for a microscope or waveguide geometry[31,32]), however, due to only one of the field interactions in the sequence being phase modulated, n = 2 2D-IR signals are eliminated using the four-frame phase cycle of Eq. (3).

Fifth-order signals involving three probe interactions (defined here as n = 3 2D-IR) are depicted schematically in Fig. 7. Unlike the third-order n = 2 processes considered above, these diagrams feature time-ordered pulse sequences where a population state separates the pump and probe interactions. They are, therefore, not eliminated through pump beam phase cycling nor by phase matching, as they radiate in the same direction of the n = 1 2D-IR signal in the pump-probe geometry. Fifth-order n = 3 processes manifest in a 2D spectrum as extra absorptions in a similar manner to the more common situation where the pump beam induces fifth-order transitions.[43] n = 3 probe effects are, therefore, relevant in a bright probe experiment under limiting cases of systems of strong transition dipole moment (e.g., metal-carbonyls), high pulse energies, and tight focusing. At the 0.5–1 μJ pulse energies used here, fifth-order effects are typically weak. Looking closely at the 2D-IR spectrum of TiO_2 in Fig. 5(a), there is evidence for fifth-order effects. These are shown more fully in supplementary material, Sec. 4. With pump and probe pulses of comparable intensity, both beams could be contributing. In the three-pulse pump-probe arrangement, fifth-order signals vary quadratically with the energy of either pump or probe pulses, and hence, they can be straightforwardly eliminated without much loss in third-order signal or bright probe scatter suppression simply by lowering both the pump and probe intensities until they are no longer present.

Heating and thermal transients

In this section, we discuss the effects of laser heating and other sources of temperature uncertainties associated with 2D-IR spectroscopic measurements of pelleted solid samples. Pulsed and steady state laser heating is not typically a consideration for 1–10 kHz rate solution phase 2D-IR spectroscopy, except when solvents of low heat capacity and low thermal conductance are studied close to their boiling points. Aqueous samples in thermal contact with optical windows cool on tens of microseconds timescales;[44] hence, high repetition rate (100 kHz) liquid phase measurements do require an estimation of laser heating effects.[35,36] The cooling time of the free-standing solid samples in air studied here was found by pump-probe spectroscopy to be milliseconds. For the 10 kHz laser system used for 2D-IR measurements, laser heating, therefore, has to be taken into account.

The steady-state temperature of a sample within the focus of 2D-IR pump and probe beams can be estimated by comparing temperature-dependent FT-IR difference spectra of the sample with difference spectra calculated from 2D-IR probe laser transmission measurements taken with pump light and without pump light. An example measurement is shown in Fig. 8 for a pellet of ZSM-5
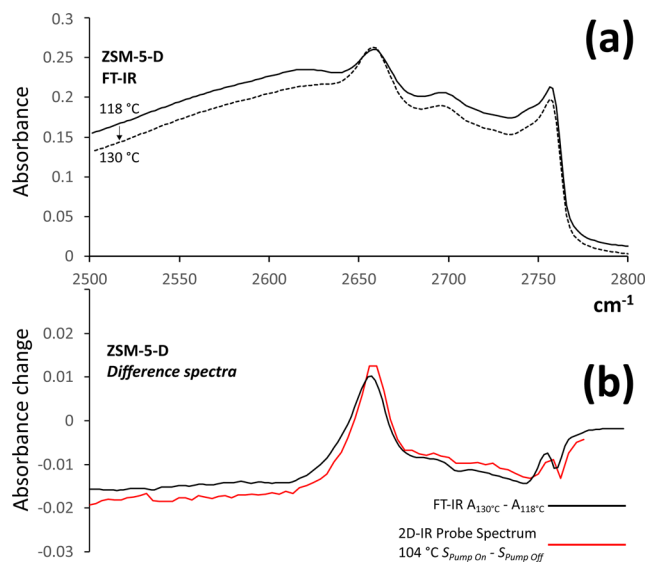

FIG. 8. Assessing steady-state laser heating in 2D-IR experiments. (a) FT-IR spectra of a zeolite (ZSM-5) pellet at 118 and 130 °C. (b) The FT-IR difference spectrum of (a) matches the absorbance change of transmitted probe light through ZSM-5 held at 104 °C for successive averages of the 2D-IR probe intensity with and without the 2D-IR pump light.

(~100 μm thickness) in flowing N_2/D_2O vapor mounted across the central hole of a Linkam cell heating block and, therefore, exposed directly to the gas stream. Figure 8(a) shows how the deuterated ZSM-5 FT-IR spectrum changes between cell set point temperatures of 118 and 130 °C. This sample has a total absorption of 0.2–0.25 (optical density). The difference spectra in Fig. 8(b) reveal a prominent change at 2660 cm^{-1} from the zeolite's acid site OD stretch, which gains strength as water is removed from the hotter sample. There is a broad loss of other hydrogen-bonded species and a temperature-dependent frequency shifting of the SiOD stretch at 2760 cm^{-1}.

The difference FT-IR spectra calculated from Fig. 8(a) match 2D-IR probe laser difference spectra, shown in Fig. 8(b) when the latter measurement is conducted at a 104 °C sample base temperature. This was measured from the same sample irradiated by ~5 mW of probe light (focused to around 50 μm at the sample) with and without ~4 mW of overlapped, focused, pump light. A long waiting time (t_2 = 150 ps), crossed polarization, and bright probe eliminated scatter effects from the measurement. We can conclude that the 10 kHz pump pulse train heats the ZSM-5 sample by ~12 °C. By the lower overall cell set-point of the 2D-IR probe transmission measurement, we infer that the probe heated the sample by ~14 °C. In a 2D-IR experiment, the application of the pulse shaper masks required for pulse pair generation reduces the incident pump power levels by 40% compared with Fig. 8. Then, the total temperature increase due to the pump and probe light at the laser focus for a 2D-IR measurement is, therefore, ~21 °C ± 25%. The margin of error is an estimate from the qualitative match of the difference spectra.

Presenting the pellet to the lasers and gas-stream unsupported has the advantage of a quick equilibration of the sample to changes

in cell temperature and gas stream. We observe that holding a pellet tightly between CaF_2 windows allows more efficient conduction of deposited laser heat from the sample, dropping the steady-state temperature of the sample in the laser spot by a factor of 2–2.5×. In addition to laser heating, heating geometries (such as the Linkam arrangement used) involving direct sample contact with a heater block and optical transmission through an aperture in the center of the heater were observed to exhibit substantial temperature gradients across the aperture—an additional uncertainty. Prior to any 2D-IR measurements, we therefore had to determine the actual temperatures of the samples using an IR camera. This is described in more detail in supplementary material, Sec. 5. For a given sample type and cell geometry, this calibration process only needs to be conducted once. For the zeolite samples studied in the Linkam arrangement, we observed a sharp drop in temperature around the aperture, with a uniformly lower temperature across the aperture. The center of the pellet had a temperature of around 75% of the heater block temperature when free-standing, and 85% of the heater block when held in direct contact with CaF_2 windows.

The pulsed nature of 2D-IR measurements means that steady-state temperature rises in the sample at the laser focus are accompanied by periodic/transient temperature modulation. This introduces a modulation on the diagonal of the 2D-IR spectrum, reported for 100 kHz 2D-IR spectroscopy by Farrell et al.[36] and in IR pump-probe experiments by Schanz et al.[45] These works identified the relevant effects as signals from pump-induced thermal lenses and pump-probe induced thermal gratings persisting from one laser shot to the next. Although this effect will often be masked by the strong diagonal scatter of pelleted solids, for ⟨XXYY⟩ measurements with minimal scatter, we observed this effect for self-supporting zeolites to be relatively strong (at peak, 50% of the diagonal signal) but limited to waiting times <0.4–0.6 ps. The effect looks similar to scatter but is dispersive in anti-diagonal shape. We provide further information about this effect and some examples in supplementary material, Sec. 6.

CONCLUSION

In this work, we have presented scatter-free 2D-IR spectra of pelleted solids. In the form of discs of crushed, micro-structured powders, the samples studied are strongly IR scattering and, therefore, are not a form of sample commonly studied with 2D-IR spectroscopy. We argue that the successful acquisition of the 2D-IR spectra was made possible by using a bright probe, perpendicular pump-probe polarization, and pulse shaper phase cycling, and we demonstrate that even high quality parallel polarization measurements are possible, albeit accepting a component of scatter signal on-diagonal. We anticipate that with these kinds of developments of 2D-IR spectroscopy applied to the study of heterogeneous solids and catalysts, 2D-IR spectroscopy will be able to contribute in furthering the understanding of a wide range of interesting materials of both fundamental and industrial interest.

SUPPLEMENTARY MATERIAL

A supplementary material document is available containing: (1) further discussion about the relative amounts of direct and heterodyne scatter, (2) factors to consider regarding H-D isotope exchange, (3) practical guidance on locating a signal from a scattering sample, (4) evidence of fifth order signals in the P25 TiO_2 2D-IR data, (5) IR camera measurements of the sample temperature within the sample cells, (6) a description of inter-pulse thermal transient signals and a demonstration of their behavior in the 2D-IR spectra of ZSM-5 and fumed silica.

AUTHOR DECLARATIONS

Conflict of Interest

The authors have no conflicts to disclose.

Author Contributions

Paul M. Donaldson: Conceptualization (lead); Data curation (lead); Formal analysis (lead); Funding acquisition (lead); Investigation (lead); Methodology (lead); Project administration (lead); Resources (lead); Writing – original draft (lead); Writing – review & editing (lead). **Russell F. Howe**: Funding acquisition (supporting); Investigation (supporting); Methodology (supporting); Resources (supporting); Writing – review & editing (supporting). **Alexander P. Hawkins**: Investigation (supporting); Methodology (supporting); Writing – review & editing (supporting). **Mike Towrie**: Funding acquisition (supporting); Resources (supporting); Writing – review & editing (supporting). **Gregory M. Greetham**: Funding acquisition (supporting); Investigation (supporting); Methodology (supporting); Resources (supporting); Writing – review & editing (supporting).

DATA AVAILABILITY

The data that supports the findings of this study are available from the corresponding author upon reasonable request.

REFERENCES

[1] J. Haber, J. H. Block, and B. Delmon, "Methods and procedures for catalyst characterization," in *Handbook of Heterogeneous Catalysis* (John Wiley & Sons, 2008), pp. 1230–1258.

[2] B. M. Weckhuysen, "Preface: Recent advances in the *in situ* characterization of heterogeneous catalysts," Chem. Soc. Rev. **39**, 4557–4559 (2010).

[3] S. Bordiga, C. Lamberti, F. Bonino, A. Travert, and F. Thibault-Starzyk, "Probing zeolites by vibrational spectroscopies," Chem. Soc. Rev. **44**, 7262–7341 (2015).

[4] F. Zaera, "New advances in the use of infrared absorption spectroscopy for the characterization of heterogeneous catalytic reactions," Chem. Soc. Rev. **43**, 7624–7663 (2014).

[5] A. Savara and E. Weitz, "Elucidation of intermediates and mechanisms in heterogeneous catalysis using infrared spectroscopy," Annu. Rev. Phys. Chem. **65**, 249–273 (2014).

[6] J. J. Bravo-Suárez and P. D. Srinivasan, "Design characteristics of *in situ* and operando ultraviolet-visible and vibrational spectroscopic reaction cells for heterogeneous catalysis," Catal. Rev.: Sci. Eng. **59**(4), 295–445 (2017).

[7] P. Hamm and M. Zanni, *Concepts and Methods of 2D Infrared Spectroscopy* (Cambridge University Press, 2011), Vol. 9781107000.

[8] J. P. Kraack and P. Hamm, "Surface-sensitive and surface-specific ultrafast two-dimensional vibrational spectroscopy," Chem. Rev. **117**(16), 10623–10664 (2017).

[9] A. Tokmakoff, "Two-dimensional line shapes derived from coherent third-order nonlinear spectroscopy," J. Phys. Chem. A **104**(18), 4247–4255 (2000).

[10] N. Demirdöven, M. Khalil, and A. Tokmakoff, "Correlated vibrational dynamics revealed by two-dimensional infrared spectroscopy," Phys. Rev. Lett. **89**(23), 237401 (2002).

[11] J. B. Asbury, T. Steinel, K. Kwak, S. A. Corcelli, C. P. Lawrence, J. L. Skinner, and M. D. Fayer, "Dynamics of water probed with vibrational echo correlation spectroscopy," J. Chem. Phys. **121**(24), 12431–12446 (2004).

[12] S. T. Roberts, K. Ramasesha, and A. Tokmakoff, "Structural rearrangements in water viewed through two-dimensional infrared spectroscopy," Acc. Chem. Res. **42**(9), 1239–1249 (2009).

[13] M. C. Thielges, J. K. Chung, and M. D. Fayer, "Protein dynamics in cytochrome P450 molecular recognition and substrate specificity using 2D IR vibrational echo spectroscopy," J. Am. Chem. Soc. **133**(11), 3995–4004 (2011).

[14] K. Ramasesha, S. T. Roberts, R. A. Nicodemus, A. Mandal, and A. Tokmakoff, "Ultrafast 2D IR anisotropy of water reveals reorientation during hydrogen-bond switching," J. Chem. Phys. **135**(5), 054509 (2011).

[15] D. V. Kurochkin, S. R. G. Naraharisetty, and I. V. Rubtsov, "A relaxation-assisted 2D IR spectroscopy method," Proc. Natl. Acad. Sci. U. S. A. **104**(36), 14209–14214 (2007).

[16] B. L. McClain, I. J. Finkelstein, and M. D. Fayer, "Vibrational echo experiments on red blood cells: Comparison of the dynamics of cytoplasmic and aqueous hemoglobin," Chem. Phys. Lett. **392**(4–6), 324–329 (2004).

[17] S.-H. Shim and M. T. Zanni, "How to turn your pump–probe instrument into a multidimensional spectrometer: 2D IR and vis spectroscopiesvia pulse shaping," Phys. Chem. Chem. Phys. **11**(5), 748–761 (2009).

[18] R. Bloem, S. Garrett-Roe, H. Strzalka, P. Hamm, and P. Donaldson, "Enhancing signal detection and completely eliminating scattering using quasi-phase-cycling in 2D IR experiments," Opt. Express **18**(26), 27067 (2010).

[19] J. Helbing and P. Hamm, "Compact implementation of Fourier transform two-dimensional IR spectroscopy without phase ambiguity," J. Opt. Soc. Am. B **28**(1), 171 (2011).

[20] J. Réhault and J. Helbing, "Angle determination and scattering suppression in polarization-enhanced two-dimensional infrared spectroscopy in the pump-probe geometry," Opt. Express **20**(19), 21665 (2012).

[21] I. C. Spector, C. M. Olson, C. J. Huber, and A. M. Massari, "Simple fully reflective method of scatter reduction in 2D-IR spectroscopy," Opt. Lett. **40**(8), 1850 (2015).

[22] J. G. Seol, H. Kwon, G. Y. Jin, J. Moon, C. Yi, and Y. S. Kim, "Scattering elimination of heterodyne-detected two-dimensional infrared spectra using choppers and shutters," J. Phys. Chem. A **123**(50), 10837–10843 (2019).

[23] C. Yan, J. Nishida, R. Yuan, and M. D. Fayer, "Water of hydration dynamics in minerals gypsum and bassanite: Ultrafast 2D IR spectroscopy of rocks," J. Am. Chem. Soc. **138**(30), 9694–9703 (2016).

[24] J. Nishida and M. D. Fayer, "Guest hydrogen bond dynamics and interactions in the metal-organic framework MIL-53(Al) measured with ultrafast infrared spectroscopy," J. Phys. Chem. C **121**(21), 11880–11890 (2017).

[25] J. H. Hack, J. P. Dombrowski, X. Ma, Y. Chen, N. H. C. Lewis, W. B. Carpenter, C. Li, G. A. Voth, H. H. Kung, and A. Tokmakoff, "Structural characterization of protonated water clusters confined in HZSM-5 zeolites," J. Am. Chem. Soc. **143**(27), 10203–10213 (2021).

[26] J. Nishida, A. Tamimi, H. Fei, S. Pullen, S. Ott, S. M. Cohen, and M. D. Fayer, "Structural dynamics inside a functionalized metal-organic framework probed by ultrafast 2D IR spectroscopy," Proc. Natl. Acad. Sci. U. S. A. **111**(52), 18442–18447 (2014).

[27] M. Bonn, H. J. Bakker, A. W. Kleyn, and R. A. van Santen, "Dynamical studies of zeolite protons and interactions with adsorbates by picosecond infrared spectroscopy," Appl. Surf. Sci. **121-122**, 80–88 (1997).

[28] T. Fujino, M. Kashitani, K. Fukuyama, J. Kubota, J. N. Kondo, A. Wada, K. Domen, C. Hirose, F. Wakabayashi, and S. S. Kano, "Population lifetimes of the OH stretching band of water molecules on zeolite surfaces," Chem. Phys. Lett. **261**(4–5), 534–538 (1996).

[29] I. P. Clark and M. Towrie, "A compact micro-bolometer array for mid-infrared laser beam alignment, diagnostics and spot-size measurement," Preprints **2019**, 2019120085.

[30] Y. Feng, I. Vinogradov, and N.-H. Ge, "General noise suppression scheme with reference detection in heterodyne nonlinear spectroscopy," Opt. Express **25**(21), 26262 (2017).

[31] G. M. Greetham, I. P. Clark, D. Weidmann, M. N. R. Ashfold, A. J. Orr-Ewing, and M. Towrie, "Waveguide-enhanced 2D-IR spectroscopy in the gas phase," Opt. Lett. **38**(18), 3596 (2013).

[32] C. R. Baiz, D. Schach, and A. Tokmakoff, "Ultrafast 2D IR microscopy," Opt. Express **22**(15), 18724 (2014).

[33] N. M. Kearns, R. D. Mehlenbacher, A. C. Jones, and M. T. Zanni, "Broadband 2D electronic spectrometer using white light and pulse shaping: Noise and signal evaluation at 1 and 100 KHz," Opt. Express **25**(7), 7869 (2017).

[34] B. M. Luther, K. M. Tracy, M. Gerrity, S. Brown, and A. T. Krummel, "2D IR spectroscopy at 100 KHz utilizing a mid-IR OPCPA laser source," Opt. Express **24**(4), 4117 (2016).

[35] P. M. Donaldson, G. M. Greetham, D. J. Shaw, A. W. Parker, and M. Towrie, "A 100 KHz pulse shaping 2D-IR spectrometer based on dual Yb:KGW amplifiers," J. Phys. Chem. A **122**(3), 780–787 (2018).

[36] K. M. Farrell, J. S. Ostrander, A. C. Jones, B. R. Yakami, S. S. Dicke, C. T. Middleton, P. Hamm, and M. T. Zanni, "Shot-to-shot 2D IR spectroscopy at 100 KHz using a Yb laser and custom-designed electronics," Opt. Express **28**(22), 33584 (2020).

[37] A. M. Horst, A. C. Neal, R. E. Mielke, P. R. Sislian, W. H. Suh, L. Mädler, G. D. Stucky, and P. A. Holden, "Dispersion of TiO₂ nanoparticle agglomerates by *Pseudomonas aeruginosa*," Appl. Environ. Microbiol. **76**(21), 7292–7298 (2010).

[38] H. Barthel, M. Heinemann, M. Stintz, and B. Wessely, "Particle sizes of fumed silica," Part. Part. Syst. Charact. **16**(4), 169–176 (1999).

[39] P. M. Donaldson, "Spectrophotometric concentration analysis without molar absorption coefficients by 2D-IR and FT-IR spectroscopy," Anal. Chem. **94**(51), 17988–17999 (2022).

[40] H. Lin, J. Long, Q. Gu, W. Zhang, R. Ruan, Z. Li, and X. Wang, "*In situ* IR study of surface hydroxyl species of dehydrated TiO₂: Towards understanding pivotal surface processes of TiO₂ photocatalytic oxidation of toluene," Phys. Chem. Chem. Phys. **14**, 9468–9474 (2012).

[41] P. M. Donaldson, A. P. Hawkins, G. M. Greetham, and R. F. Howe, "New insights into framework and water and hydroxyl groups in acid zeolites from two-dimensional infrared spectroscopy" (unpublished).

[42] K. M. Farrell and M. T. Zanni, "Phase stable, shot-to-shot measurement of third- and fifth-order two-quantum correlation spectra using a pulse shaper in the pump-probe geometry," J. Chem. Phys. **157**(1), 014203 (2022).

[43] S. M. Arrivo, T. P. Dougherty, W. T. Grubbs, and E. J. Heilweil, "Ultrafast infrared spectroscopy of vibrational CO-stretch up-pumping and relaxation dynamics of W(CO)₆," Chem. Phys. Lett. **235**(3–4), 247–254 (1995).

[44] G. M. Greetham, I. P. Clark, B. Young, R. Fritsch, L. Minnes, N. T. Hunt, and M. Towrie, "Time-resolved temperature-jump infrared spectroscopy at a high repetition rate," Appl. Spectrosc. **74**(6), 720–727 (2020).

[45] R. Schanz, V. Boţan, and P. Hamm, "A femtosecond study of the infrared-driven *cis-trans* isomerization of nitrous acid (HONO)," J. Chem. Phys. **122**(4), 044509 (2005).